

# The gluon condensation in high energy cosmic rays

Wei Zhu<sup>1\*</sup>, Jiangshan Lan<sup>2</sup> and Jianhong Ruan<sup>1</sup>

<sup>1</sup>Department of Physics, East China Normal University, Shanghai 200241, China

<sup>2</sup>Institute of Modern Physics, Chinese Academy of Sciences, Lanzhou 730000, China

## Abstract

The gluon condensation (GC)-effects in high energy cosmic rays are investigated. After a brief review of the GC, several examples including gamma-, electron-, and positron-spectra in a broad GeV~TeV region can be explained by the GC-effects. We find that the GC may break the power-law of the cosmic ray spectra if the energy of accelerated protons exceeds the GC-threshold. The GC is a new phenomenon that is not yet known, it provides a new window to understand the high energy cosmic ray spectra.

**keywords:** Quantum Chromodynamics; Gluon condensation; Cosmic ray spectra

**PACS numbers:**12.38.-t; 14.70.Dj; 14.20.Dh; 95.30.Cq

---

\*Corresponding author, E-mail: weizhu@mail.ecnu.edu.cn

# 1 Introduction

The majority of high energy particles in cosmic rays are protons. Proton-proton (or nuclei) ( $p-p(A)$ ) collisions are general events in Universe. Gluons inside proton dominate the proton collisions at high energy and their distributions obey the evolution equations based on Quantum Chromodynamics (QCD). QCD analysis shows that the evolution equations will become nonlinear due to the initial gluons correlations at high energy and these will result in the chaotic solution beginning at a threshold energy [1,2]. Most surprisingly, the dramatic chaotic oscillations produce strong shadowing and antishadowing effects, they converge gluons to a state at a critical momentum [3]. This is the gluon condensation (GC) in proton. We will give a brief review about its history in Sec. 2.

The GC-effects should induce significant effects in the proton processes, provided the GC-threshold  $E_{p-p(A)}^{GC}$  enters the observable high energy region. Unfortunately, the exact value of  $E_{p-p(A)}^{GC}$  can not be entirely determined in theory since it relates to the unknown input conditions. On the other hand, we have not observed the GC-effects until 13 TeV in  $p-p$  collisions and 5 ~ 8 TeV in  $Pb-Pb$  collisions at the Large Hadron Collider (LHC). Therefore, we turn to study the energy spectra of high energy cosmic rays. Protons accelerated in the Universe may exceed  $E_{p-p(A)}^{GC}$  and cause the GC-effects in their collisions.

The power-law form of energy spectrum is a general rule of the cosmic ray spectra at high energy. It is described by a straight line of the energy spectrum with a fixed index in a log-log representation. This line may span over more than one order of magnitude. The broken power-law relates to the extra sources of cosmic rays or vent a new effect. We noticed that there are different radiation mechanisms. Usually even one  $\gamma$ -ray spectrum may arise the arguments of leptonic or hadronic explanations. Therefore, we ask what is the GC-characteristic spectrum? Can it distinguish the GC-effects from other

phenomena? We will discuss the above questions at Sec. 3.

Following the results of Sec.3, we calculate the gamma spectrum of a supernova remnant (SNR) Tycho [4] in Sec. 4. We assume that the protons accelerated in this SNR may exceed  $E_{p-p(A)}^{GC}$  ( $A$  indicates the nucleon number of a targeted nucleus). Thus, the GC-effects dominate their energy spectra if accelerated protons interact with the surrounding dense matter inside the source. We find that our predicted sharp broken power-law is consistent with the observed data. Following this example, a several sharp broken power examples of the gamma ray originating from SNRs and Active Galactic Nuclei (AGN) are discussed.

An excess of the cosmic ray positron spectra at 10 GeV-1 TeV has been reported by the Alpha Magnetic Spectrometer (AMS02) [5], which was interpreted as the DM-signature. A similar excess structure in the electron-positron spectrum at 300 GeV-700 GeV was early reported by the Advanced Thin Ionization Calorimeter (ATIC) [6]. However, the later finding was not confirmed by more accurate observations of the the Fermi Large Area Telescope (Fermi-LAT) [7], the High Energy Stereoscopic System (H.E.S.S.) [8,9], the Major Atmospheric Gamma Imaging Cherenkov (MAGIC) [10] and the VERITAS [11]. The new data show that a smooth broken power in the electron energy spectrum may expand to a broader range rather than a narrow excess. We try to explain these results using the GC-effects in Sec. 5. Finally, a summary is given in Sec. 6.

$$\begin{aligned}
Q^2 \frac{\partial G(x, Q^2)}{\partial Q^2} &= \frac{\alpha_s N_c}{\pi} \int_x^1 \frac{dx_1}{x_1} G(x_1, Q^2) & -x \frac{\partial F(x, \underline{k}_{a0})}{\partial x} \\
& & = \frac{\alpha_s N_c}{2\pi^2} \int d^2 k_{ab} \frac{k_{a0}^2}{k_{ab}^2 k_{0b}^2} [2F(x, \underline{k}_{ab}) - F(x, \underline{k}_{a0})] \\
\text{DGLAP} & & \text{BFKL} \\
\frac{\partial G(x, Q^2)}{\partial \ln Q^2} & & -x \frac{\partial N(\underline{k}^2, x)}{\partial x} \\
& = \frac{\alpha_s N_c}{\pi} \int_x^1 \frac{dx_1}{x_1} G(x_1, Q^2) & = \frac{\alpha_s N_c}{\pi} \int_{k_{min}^2}^{\infty} \frac{dk'^2}{k'^2} \frac{k'^2 N(k'^2, x) - k^2 N(k^2, x)}{|k'^2 - k^2|} \\
& + \frac{9\alpha_s^2}{2\pi R_N^2 Q^2} \frac{N_c^2}{N_c^2 - 1} \int_{x/2}^{1/2} \frac{dx_1}{x_1} G^2(x_1, Q^2) & + \frac{\alpha_s N_c}{\pi} \int_{k_{min}^2}^{\infty} \frac{dk'^2}{k'^2} \frac{k^2 N(k^2, x)}{\sqrt{k^4 + 4k'^4}} - \frac{\alpha_s N_c}{\pi} N^2(k^2, \frac{x}{2}) \\
& - \frac{9\alpha_s^2}{\pi R_N^2 Q^2} \frac{N_c^2}{N_c^2 - 1} \int_x^{1/2} \frac{dx_1}{x_1} G^2(x_1, Q^2) & \\
\text{GLR-MQ-ZRS} & & \text{BK}
\end{aligned}$$

Figure 1: A set of the QCD evolution equations for gluons at small  $x$  and leading order approximation. Where the BK equation is taken in a full momentum space.  $G(x, Q^2)$  and  $F(x, \underline{k})$  are integrated and unintegrated gluon distributions.

## 2 A brief review about the gluon condensation

The QCD evolution equations have different forms at different energy ranges. At high energy, or small Bjorken variable  $x$ , gluon distributions dominate the evolution processes (Fig. 1) according to the linear DGLAP (Dokshitzer-Gribov-Lipatov-Altarelli-Parisi) equation [12-14] and BFKL (Balitsky-Fadin-Kuraev-Lipatov) equation [15-19]. They both predict that the gluon density in proton grows with decreasing  $x$  and it will cause the violation of the unitarity of the scattering cross section. In consequence, a series of the nonlinear evolution equations, for example, the GLR-MQ-ZRS (Gribov-Levin-Ryskin, Mueller-Qiu, Zhu-Ruan-Shen) equation [20-24] and BK (Balitsky-Kovchegov) equation [25,26] were proposed, in which the corrections of gluon recombination are considered. An important result of the non-linearization is that the BK equation, or its generalization, the Jalilian-Marian-Iancu-McLerran-Weigert-Leonidov-Kovner (JIMWLK) equation [27-29], predicts the unintegrated gluon distribution  $F(x, \underline{k}) \rightarrow$  a constant when the transverse momentum  $\underline{k}$  of gluon is smaller than a characteristic saturation momentum  $Q_s(x)$ . This saturation

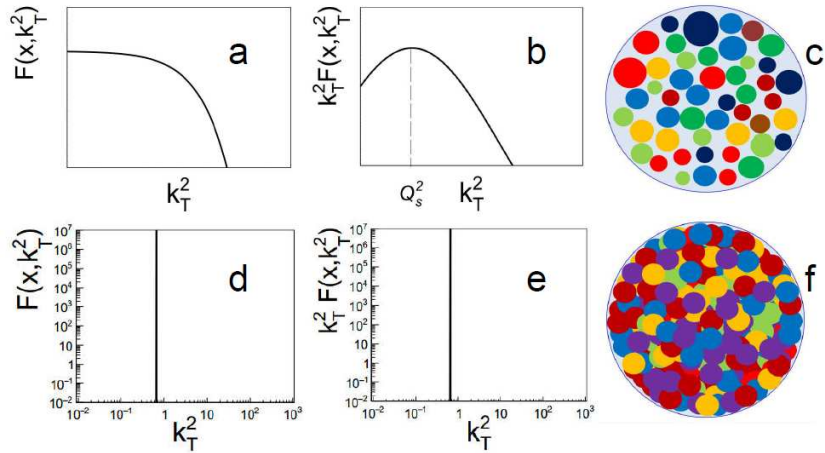


Figure 2: Schematic diagrams (a-c) for the saturation solutions of the BK/JIMWLK equation; (d-f) for the condensation solutions of the ZSR equation, which is evolved with the GBW input.

behavior implies a balance between gluon splitting and fusion, however it is also understood as the color glass condensate (CGC), where “condensate” implies that the maximum occupation number of gluons is  $\sim 1/\alpha_s > 1$ , although it lacks a characteristic sharp peak in the momentum distribution (Fig. 2 (a-c)).

A new nonlinear evolution equation based on Fig. 3 is derived by Zhu, Shen and Ruan (ZSR) in works [1,2]. According to the standard quantum field theory, summing-up all possible amplitudes including so-called virtual processes are necessary for the regularization of the evolution equations. The derivation of the nonlinear evolution equations based on Fig. 3 includes the contributions from real 2-2, virtual 2-2, real 1-3 and virtual 1-3 amplitudes. A key point is how to calculate the above complicated virtual diagrams? Fortunately, such a technique was established using the time ordered perturbation theory (TOPT) in work [22]. This TOPT-cutting rule was successfully used to recover the momentum non-conservation in the GLR-MQ equation [23] and obtained the support in

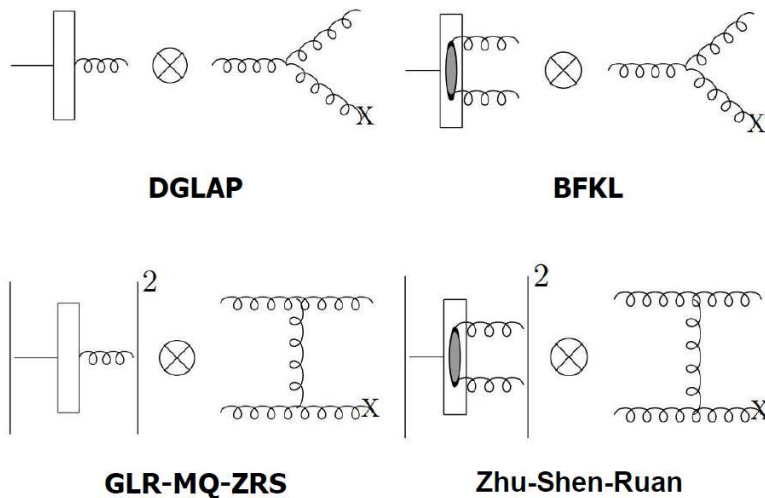


Figure 3: A set of consistent elemental amplitudes. Note that a complete evolution equation based on (d) should contain interference and virtual processes. These four evolution equations were unitary derived using the time ordered perturbative theory in [1,2].

serious of examples [30-35]. Using the TOPT cutting rule, the resulting ZSR equation for the unintegrated gluon distribution  $F(x, \underline{k}^2)$  at the leading logarithmic ( $LL(1/x)$ ) approximation is [2]

$$\begin{aligned}
 & -x \frac{\partial F(x, \underline{k}^2)}{\partial x} \\
 &= \frac{3\alpha_s \underline{k}^2}{\pi} \int_{\underline{k}_0^2}^{\infty} \frac{d\underline{k}'^2}{\underline{k}'^2} \left\{ \frac{F(x, \underline{k}'^2) - F(x, \underline{k}^2)}{|\underline{k}'^2 - \underline{k}^2|} + \frac{F(x, \underline{k}^2)}{\sqrt{\underline{k}^4 + 4\underline{k}'^4}} \right\} \\
 & - \frac{81}{16} \frac{\alpha_s^2}{\pi R_N^2} \int_{\underline{k}_0^2}^{\infty} \frac{d\underline{k}'^2}{\underline{k}'^2} \left\{ \frac{\underline{k}^2 F^2(x, \underline{k}'^2) - \underline{k}'^2 F^2(x, \underline{k}^2)}{\underline{k}'^2 |\underline{k}'^2 - \underline{k}^2|} + \frac{F^2(x, \underline{k}^2)}{\sqrt{\underline{k}^4 + 4\underline{k}'^4}} \right\}, \quad (1)
 \end{aligned}$$

where the first item on the right is the BFKL equation part and the second one is nonlinear correction caused by the gluon fusions. The singular structure in the linear and nonlinear evolution kernels both corresponds to the random evolution in the  $\underline{k}$ -space, where  $\underline{k}^2 - \underline{k}'^2$  may cross over zero. This is a general property of the logarithmic ( $1/x$ ) resummation, and remember, this is also a key point of our following work.

It is interesting that the nonlinear ZSR evolution equation results in the chaotic solution if the Bjorken variable  $x$  goes beyond a critical point  $x_c$ . This is a chaotic example in the QCD evolution equations, although chaos is a popular natural phenomenon in nonlinear science. Most surprisingly, the dramatic chaotic oscillations produce the strong shadowing and antishadowing effects via the nonlinear terms of Eq. (1), they converge gluons to a state with a critical momentum (Figs. 2(d-f)). This is the gluon condensation (GC) in proton (see Fig. 4(a), for comparison, we present the GBW model in Fig. 4(b), which describes the CGC solution).

We emphasize that the above chaotic solution or the convergence effect originates from the regularized nonlinear part in Eq. (1), and it is a general structure of the logarithmic ( $1/x$ ) resummation even at higher ordered approximations. One can understand this point as follows.

(i) The gluon transverse momentum after the above mentioned splitting process may be either larger or smaller than that of the primary gluon. As we know that the contributions of evolution along a random chain of gluon-transverse momentum  $\underline{k}$  are important at high energy. This point is always emphasized by the classical linear BFKL evolution equation, unfortunately, it was neglected, or is purposely avoided by other nonlinear QCD evolution equations. Comparing with the BK-JIMWLK equations, the ZSR equation (1) keeps the regularized nonlinear terms and they have the derivative structure  $\sim \partial F(x, \underline{k}^2)/\partial \underline{k}^2$  and  $\sim \partial F^2(x, \underline{k}^2)/\partial \underline{k}^2$  in Eq. (1). These terms may add a perturbation on the smooth curve  $F(x, \underline{k}^2)$  once  $|\underline{k}|$  crosses over  $Q_s$ . Thus, we have a series of independent perturbations in a narrow  $|\underline{k}|$  domain near  $Q_s$  along evolution to smaller  $x$ . In the linear BFKL equation, these perturbations are independent and their effects are negligibly small. In this case the solutions keep the smooth curves in  $(x, \underline{k}^2)$  space. However, the nonlinear Eq. (1) may form chaos near  $Q_s$ . The positive Lyapunov

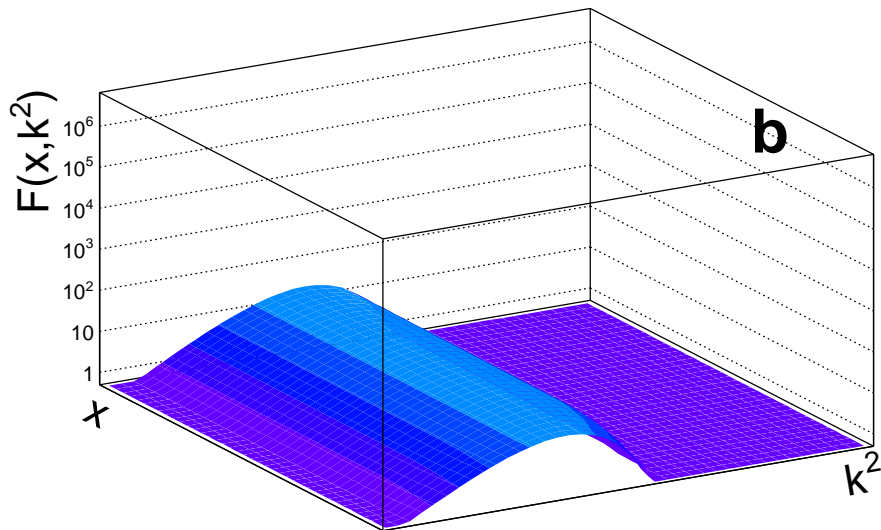
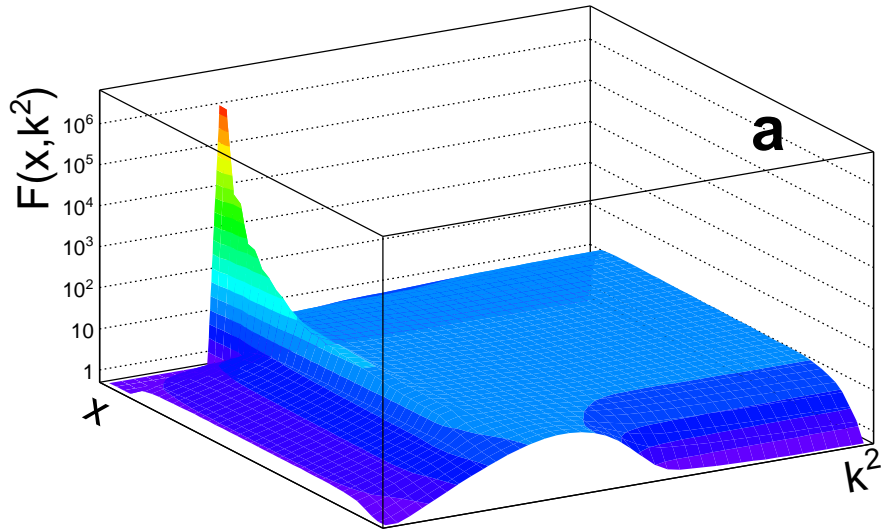


Figure 4: (a) A GC-solution of the ZSR equation; (b) The GBW input distribution.



exponents of Eq. (1) support this suggestion.

(ii) Note that once chaos is produced, the fast oscillations of the gluon density produce both the negative and positive nonlinear corrections to  $\Delta F(x, \underline{k}^2)$  through the derivative structure of Eq. (1). The former shadows the grownup of the gluon density, while the later is the antishadowing effect, and it increases rapidly the gluon density because it is a strong positive feedback process. They will result in a pair of closer and more stronger positive and negative corrections at a next evolution step, where the positive correction continually put  $F(x, \underline{k}^2)$  toward a bigger value, while the negative one suppress all remaining distributions. Thus, we observed the gluons condensation at  $(x_c, \underline{k}_c^2)$  due to the extrusion of the shadowing and antishadowing effects in the QCD evolution. (see [2,3] for details).

Equation (1) is based on the leading QCD approximation, where the higher order corrections are neglected. An important question is: will the chaos effects disappear in the evolution equation after considering higher order corrections? In other words, what is the source of the GC-effects? and will this source disappear due to the higher order corrections? We discuss them from two aspects.

(i) We have known that chaos in Eq. (1) origins from the BFKL-singularity of the non-linear evolution kernel. From the experiences in the study of the BFKL equation, higher order QCD corrections can not remove the singularities at the lower order approximation. In general case, the infrared (IR) divergence in a Feynman diagram at a given order can only be regularized by using the virtual diagrams at the same order. We divide the higher order corrections into two kinds: without and with the new IR-divergences. We have examined in works [2,3] that the former can not remove the chaos-GC solutions in Eq. (1), while the later may generate the multi-chaos. Interestingly, these multi-chaos may combine into a single chaos in the ZSR equation. Therefore, we believe that chaos-GC

effects still exist in Eq. (1) even considering the higher order corrections

(ii) We discuss the chaotic solution of Eq. (1) from the view point of the chaos theory.

It is well known that some of chaotic attractors are unstable. A slight fluctuation of a parameter may drive the system out of chaos. However, it has been proved that some dynamical systems can exhibit robust chaos. A chaotic attractor is said to be robust if, for its parameter values, there exist a neighborhood in the parameter space with absence of periodic negative Lyapunov exponents. Robustness implies that the chaotic behavior cannot be destroyed by arbitrarily small perturbations of the system parameters. The structure of the Lyapunov exponents shows that chaos in Eq. (2.1) is robust [2]. The corrections from the higher order processes cannot cancel the GC-effects.

We presented the above two reasons to support the GC-effects due to the special structure of the ZSR equation, although we can't derive a complete modified ZSR equation, which should include all order corrections. In this case, the evidence from the experiments become important. Therefore, a following question is where we can observed the GC-effects? We will discuss the GC-effects at high energy cosmic rays in the following sections.

### 3 The characters of the gluon condensation in cosmic ray spectra

The secondary particles in cosmic rays may origin from the hadronic precesses, for example,  $p + p(A) \rightarrow \pi + \text{others}$ . The GC increases suddenly the proton-proton or proton-nuclei cross sections. The shape of energy spectra of these secondary particles is an ideal subject to observe the GC-effects if the energy of incident proton is accelerated beyond the GC-threshold  $E_{p-p(A)} > E_{p-p(A)}^{GC}$ .

The cross section of inclusive gluon mini-jet production at high energy  $p - p$  collisions [20,22] reads

$$\frac{d\sigma_g}{d\underline{k}^2 dy} = \frac{64N_c}{(N_c^2 - 1)\underline{k}^2} \int \underline{q} d\underline{q} \int_0^{2\pi} d\phi \alpha_s(\Omega) \frac{F(x_1, \frac{1}{4}(\underline{k} + \underline{q})^2) F(x_2, \frac{1}{4}(\underline{k} - \underline{q})^2)}{(\underline{k} + \underline{q})^2 (\underline{k} - \underline{q})^2}, \quad (2)$$

where  $\Omega = \text{Max}\{\underline{k}^2, (\underline{k} + \underline{q})^2/4, (\underline{k} - \underline{q})^2/4\}$ ; The longitudinal momentum fractions of interacting gluons are fixed by kinematics:  $x_{1,2} = \underline{k}e^{\pm y}/\sqrt{s}$ .

The number of secondary particles is proportional to Eq. (2) if we neglect the mechanism of fragmentation of gluons into secondary particles. We denote that  $N_\pi(E_{p-p}, E_\pi)$  as pion number with energies  $E_\pi$  at  $p - p$  collisions;  $E_{p-p}$  is the energy of incident proton in the rest frame of targeted proton. The calculations of the pion-distributions at the  $p - p(A)$  collisions are very complicated due to the nonperturbative hadronization. For the simplification, we consider only pions as the secondary particles since the multiplicities of other particles at high energy collisions are much smaller than that of pions. Usually, these pions have smaller kinetic energy (or lower momentum) at the center-of-mass (C.M.) system and form the central region in the rapidity distribution. The maximum number of pions  $N_\pi$  at a given interaction energy corresponds to a case, that all available kinetic energies of pions at the C.M. system are almost used to create pions. It leads to  $N_\pi \sim \sqrt{s}$ . However, the data show that  $N_\pi \sim \ln s$  or  $\ln s^2$  [36]. A possible reason is that the limited

available number of gluons restricts the increase of secondaries [37]. We assume that a large number of gluons at the central region due to the GC-effects create the maximum number  $N_\pi$  of pions. We emphasize that this assumption is a simplification method rather than a necessary GC-condition. In fact, we will show that it may simplify the calculation but does not essentially change the GC-characteristic signature. Using general relativistic invariant and energy conservation, we have

$$(2m_p^2 + 2E_{p-p(A)}m_p)^{1/2} = E_{p1}^* + E_{p2}^* + N_\pi m_\pi, \quad (3)$$

$$E_{p-p(A)} + m_p = m_p\gamma_1 + m_p\gamma_2 + N_\pi m_\pi\gamma, \quad (4)$$

where  $E_{p_i}^*$  is the energy of leading proton at the C.M. system,  $\gamma_i$  are the corresponding Lorentz factors. Using the inelasticity  $K \sim 0.5$  [38], we set

$$E_{p1}^* + E_{p2}^* = \left(\frac{1}{K} - 1\right)N_\pi m_\pi, \quad (5)$$

and

$$m_p\gamma_1 + m_p\gamma_2 = \left(\frac{1}{K} - 1\right)N_\pi m_\pi\gamma. \quad (6)$$

One can easily get the solutions  $N_\pi(E_{p-p(A)}, E_\pi)$  for the  $p - p(A)$  collisions

$$\ln N_\pi = 0.5 \ln E_{p-p(A)} + a, \quad \ln N_\pi = \ln E_\pi + b, \quad \text{where } E_\pi \in [E_\pi^{GC}, E_\pi^{max}]. \quad (7)$$

The parameters

$$a \equiv 0.5 \ln(2m_p) - \ln m_\pi + \ln K, \quad (8)$$

and

$$b \equiv \ln(2m_p) - 2 \ln m_\pi + \ln K. \quad (9)$$

Equation (7) gives the relation among  $N_\pi$ ,  $E_{p-p(A)}$  and  $E_\pi^{GC}$  by one-to-one, which leads to a GC-characteristic spectrum.

## 4 The GC effects in the gamma ray spectra

Imaging a high energy proton collides with a proton or a nucleus, we have  $p + p(A) \rightarrow \pi^{\pm,0} + \text{others}$  and following  $\pi^0 \rightarrow 2\gamma$ . The corresponding gamma flux in a general hadronic framework reads

$$\Phi_\gamma(E_\gamma) = \Phi_\gamma^0(E_\gamma) + \Phi_\gamma^{GC}(E_\gamma), \quad (10)$$

$\Phi_\gamma^0(E_\gamma)$  is the background contribution and

$$\Phi_\gamma^{GC}(E_\gamma) = C_{p-p(A)} \left(\frac{E_\gamma}{E_0}\right)^{-\beta_\gamma} \int_{E_\pi^{min}}^{E_\pi^{max}} dE_\pi \left(\frac{E_{p-p(A)}}{E_{p-p(A)}^{GC}}\right)^{-\beta_p} N_\pi(E_{p-p(A)}, E_\pi) \frac{d\omega_{\pi-\gamma}(E_\pi, E_\gamma)}{dE_\gamma}, \quad (11)$$

where index  $\beta_\gamma$  and  $\beta_p$  denote the propagating loss of gamma rays and the acceleration mechanism of protons respectively;  $C_{p-p(A)}$  incorporates the kinematic factor with the flux dimension and the percentage of  $\pi^0 \rightarrow 2\gamma$ . The normalized spectrum for  $\pi^0 \rightarrow 2\gamma$  is

$$\frac{d\omega_{\pi-\gamma}(E_\pi, E_\gamma)}{dE_\gamma} = \frac{2}{\beta_\pi E_\pi} H\left[E_\gamma; \frac{1}{2}E_\pi(1 - \beta_\pi), \frac{1}{2}E_\pi(1 + \beta_\pi)\right], \quad (12)$$

$H(x; a, b) = 1$  if  $a \leq x \leq b$ , and  $H(x; a, b) = 0$  otherwise. Inserting Eq. (7) and (12) into Eq. (11), we have

$$\Phi_\gamma^{GC}(E_\gamma) = C_{p-p(A)} \left(\frac{E_\gamma}{E_\pi^{GC}}\right)^{-\beta_\gamma} \int_{E_\pi^{GC} \text{ or } E_\gamma}^{E_\pi^{GC, max}} dE_\pi \left(\frac{E_{p-p(A)}}{E_{p-p(A)}^{GC}}\right)^{-\beta_p} N_\pi(E_{p-p(A)}, E_\pi) \frac{2}{\beta_\pi E_\pi}, \quad (13)$$

where the lower-limit of the integration takes  $E_\pi^{GC}$  (or  $E_\gamma$ ) if  $E_\gamma \leq E_\pi^{GC}$  (or if  $E_\gamma > E_\pi^{GC}$ ).

In consequence,

$$E_\gamma^2 \Phi_\gamma^{GC}(E_\gamma) = \begin{cases} \frac{50C}{2\beta_p - 1} (E_\pi^{GC})^3 \left(\frac{E_\gamma}{E_\pi^{GC}}\right)^{-\beta_\gamma + 2} & \text{if } E_\gamma \leq E_\pi^{GC} \\ \frac{50C}{2\beta_p - 1} (E_\pi^{GC})^3 \left(\frac{E_\gamma}{E_\pi^{GC}}\right)^{-\beta_\gamma - 2\beta_p + 3} & \text{if } E_\gamma > E_\pi^{GC} \end{cases}. \quad (14)$$

It is the power-law with a sharp break. The break energy  $E_\gamma = E_\pi^{GC}$  is a direct result of the gluon distribution in Fig. 1, where a sharp peak divides the spectrum into two parts.

A pure power-law at  $E_\gamma < E_\pi^{GC}$  originates from a fixed lower limit  $\sim E_\pi^{GC}$  of integral in Eq. (13) and it is irrelevant to the concrete form of Eq. (7). The above two universal behaviors of  $\Phi_\gamma^{GC}$  are directly arisen from the GC-effects and they are different from all other well known smoothly radiation spectra. We regard them as the GC-character. The second power-law at  $E_\gamma > E_\pi^{GC}$  is a simplified result in Eqs. (3) and (4), where all available kinetic energies in the central region are used to create pions. We emphasize that any deformations from this power-law at  $E_\gamma > E_\pi^{GC}$  are allowed if our simplification is modified. One can compare Eq. (14) with the experiments to check the validity of the simplification. Even so, it does not change the above mentioned GC-character.

The SNRs are important gamma ray sources. There are different shapes of gamma energy spectra, which corresponds to various production mechanisms. For example, gamma rays can be generated as bremsstrahlung radiation when electrons and positrons interact with ambient matter, or as a result of inverse Compton scattering of low energy photons. Hadronic interactions can also create gamma rays. Indeed, proton-proton (or proton-nuclei and nuclei-nuclei) collisions may create  $\pi^0$  meson, which quickly decays into two gamma photons. The recent detection of the neutral pion-decay signature from two middle-aged SNRs: IC 443 and W44 has been demonstrated [39,40]. In normal case the gamma-ray spectrum  $\Phi_\gamma(E_\gamma)$  is symmetric about  $E_\gamma = m_\pi^0/2 = 67.5$  MeV. However, we will show that the GC-effects break the gamma power-law at GeV-TeV band. and induce the GC-effects in their gamma spectra.

Tycho is located in a relatively clean environment and have been studied over a wide range of energies. Cosmic ray protons accelerated in SNRs may reach the  $E_{p-p(A)}^{GC}$ -energy range and they interact with the surrounding matter inside SNR. Thus, the GC-effects

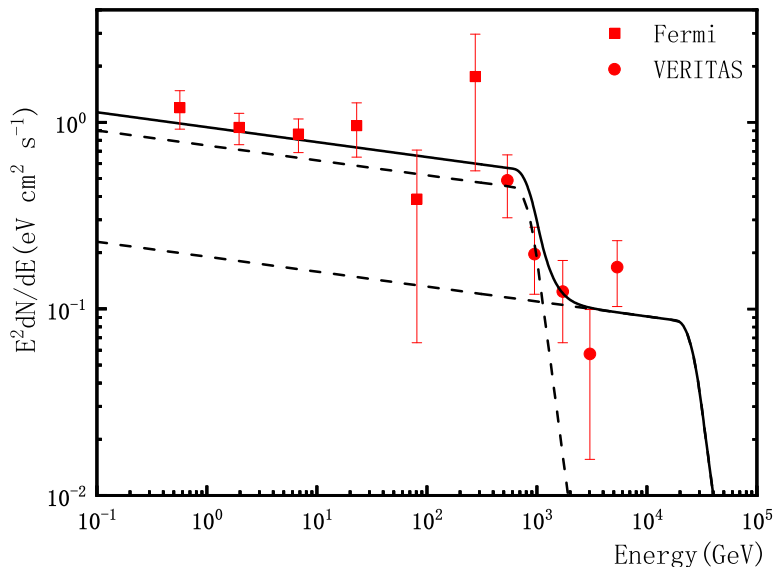


Figure 5: Predicted gamma ray spectra multiplied by  $E^2$  and comparisons with the VERITAS- and Fermi-spectrum for Tycho’s supernova remnant [4]. The broken lines are the p-A and p-p contributions, the solid line is the total contributions of the GC-effects. The parameters see Table 1.

appear in their energy spectra. Figure 5 gives our predicted gamma spectrum and the comparison with Tycho’s spectrum [4], where we take two GC-sources  $E_{\pi}^{GC} = 24$  TeV for  $p - p$  and  $E_{\pi}^{GC} = 800$  GeV for  $p - A$ . Note that  $E_{\pi}^{GC} = 24$  TeV corresponds to  $E_{p-p}^{GC} = 6 \times 10^{10}$  GeV =  $E_{GZK}$  or  $\sqrt{s_{p-p}^{GC}} = 3.3 \times 10^5$  GeV. One can find that a power-law at  $E_{\gamma} < 800$  GeV and its sharp break due to the GC-effects are significant distinction from other models. Note that we use Eq. (14) at  $E_{\gamma} > 100$  MeV where the energy loss of photons mainly origin from pairproduction. We need to consider Compton scattering and photoelectron effect at more lower energy range and change the index  $\beta_{\gamma}$ .

The sharp broken power-law was observed by Fermi-LAT and H.E.S.S. in several AGNs and SNRs. This phenomenon was explained as the emitted gamma-rays suffer from absorption by the extragalactic background light (EBL) during their travel towards Earth from the sources. However, both the distribution of EBL photons and the intrinsic VHE



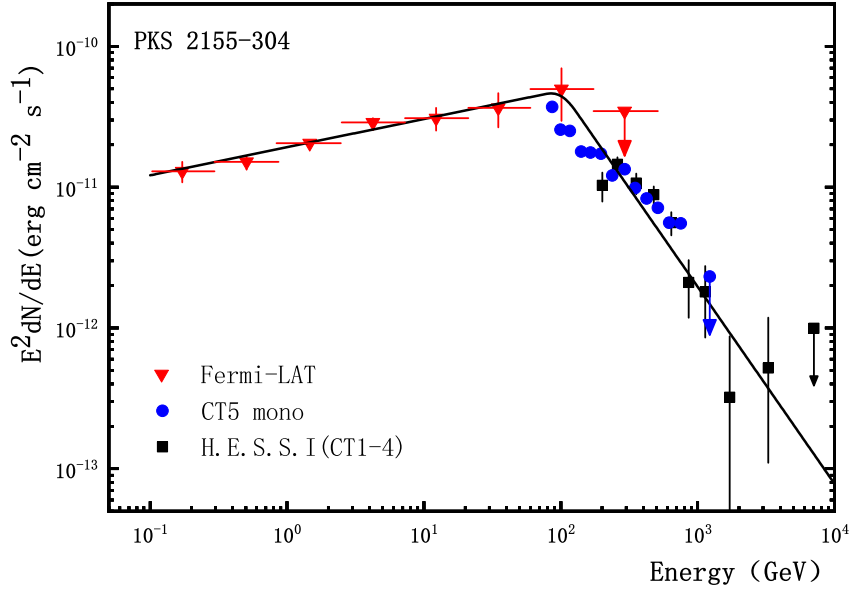


Figure 6: Predicted gamma ray spectrum multiplied by  $E^2$  and comparisons with the H.E.S.S. and Fermi-LAT spectrum for PKS 2155-304 [40]. The parameters see Table 1.

spectra of distant sources are unknown. The GC-effects provide an alternative possible explanation, where the intrinsic broken spectrum is fixed and the gamma propagating corrections including EBL absorption are described by power-law  $\sim E_\gamma^{-\beta_\gamma}$  at  $E_\gamma > 100$  GeV.

H.E.S.S. observed the high-frequency peaked of blazars PKS 2155-304 and PG 1553-113, which are among the brightest objects in the VHE gamma-ray sky [41]. Combining the spectra derived from Fermi-LAT data, the results indicate a sharp break in the observed spectra of both sources at  $E_\gamma \sim 100$  GeV. Our predicted spectra and comparisons with the data are shown in Figs.6 and 7. The parameters are listed in Table 1. The GeV gamma-ray spectrum of supernova remnants H.E.S.S. J1731-347 and SN 1006 combining Fermi-LAT data show a broken power-law once again at  $E_\gamma \sim 1$  TeV [42]. We fit it using the Eq. (14) in Fig. 8 and 9. Figures 10 and 11 are the spectra of PKS 2005-489 and

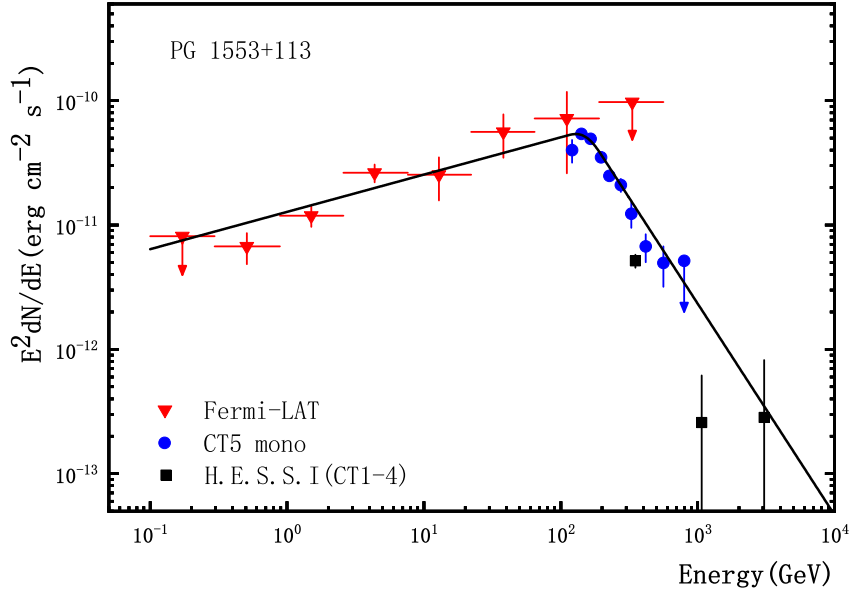


Figure 7: Predicted gamma ray spectrum multiplied by  $E^2$  and comparisons with the H.E.S.S. and Fermi-LAT spectrum for PG 1553+113 [40]. The parameters see Table 1.

Mrk 421 [43] and the comparisons with Eq. (14).

Table 1: The parameters of gamma-ray spectra.

	$E_{\pi}^{GC}(\text{GeV})$	$\beta_{\gamma}$	$\beta_p$	$C(\text{GeV}^{-2} \cdot \text{cm}^2 \cdot \text{s}^{-1})$
Tycho's SNR	800	2.08	2.70	$3.90 \times 10^{-14}$
	2400	2.08	2.70	$3.40 \times 10^{-16}$
PKS 2155-304	100	1.80	1.30	$4.80 \times 10^{-18}$
PG 1553+113	150	1.70	1.50	$2.64 \times 10^{-16}$
HESS J1731-347	800	1.70	1.00	$1.44 \times 10^{-20}$
SN 1006	300	1.70	0.82	$7.20 \times 10^{-21}$
PKS 2005-489	100	1.65	0.85	$1.35 \times 10^{-19}$
Mrk 421	200	1.50	1.00	$1.80 \times 10^{-18}$

We discuss the parameters in the above examples. Usually, the power indexes of cosmic rays spectra contains the contributions of the production mechanism and the propagation effect and they take as  $\beta_{\gamma} \sim 1.5 - 2$  and  $\beta_p \sim 2 - 3$ . Note that these values of  $\beta_p$  contains

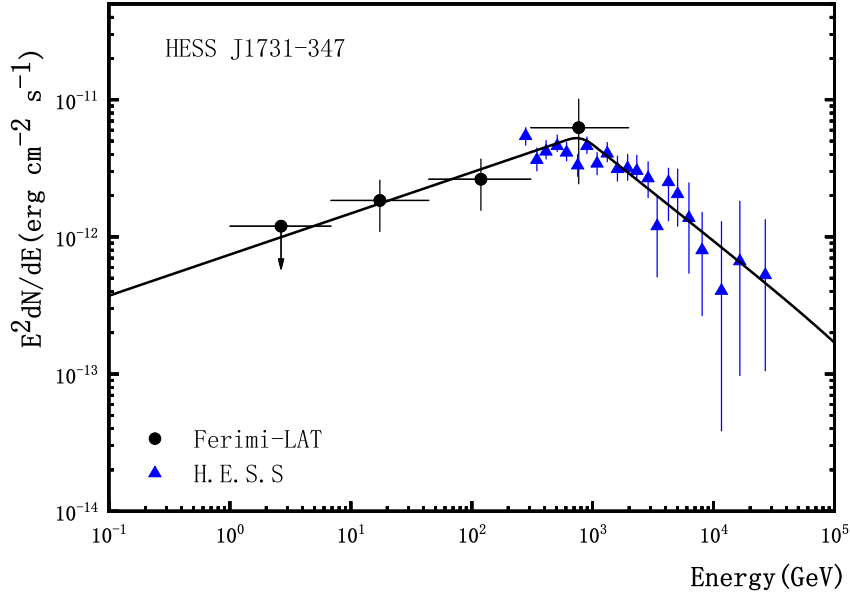


Figure 8: Predicted gamma ray spectra multiplied by  $E^2$  and comparisons with the H.E.S.S. and Fermi-LAT for J1731 [41]. The parameters see Table 1.

the interstellar propagation corrections of proton, while in this work primary protons are restricted inside the source. Therefore, the above smaller indexes are accepted.

Now we turn to the GC-threshold energy. Greisen-Zatsepin-Kuzmin (GZK) [44,45] predicted a drastic reduction of the spectrum of cosmic proton rays near the energy  $E_{GZK} \sim 6 \times 10^{19}$  eV, since the energy of the cosmic rays losses in the collisions with cosmic microwave background radiation during their long propagation. Considering that  $E_{GZK}$  is a characteristic scale, we expect that the GC- effects begin from the incident proton energy  $E_{p-p}^{GC} \equiv E_{GZK} = 6 \times 10^{19}$  eV, or  $\sqrt{s_{p-p}^{GC}} = 330$  TeV. We emphasize that this is only a possible choice and  $E_{p-p}^{GC} > E_{GZK}$  is also possible. However, it does not affect the following discussion, since there are only a few available data with large uncertainty at this energy range.

The cross section  $\sigma_{p-air}$  was derived using the distribution of the shower maximum slant depth  $X_{max}$ , where the interaction length and consequently  $\sigma_{p-air}$  relate to the  $X_{max}$

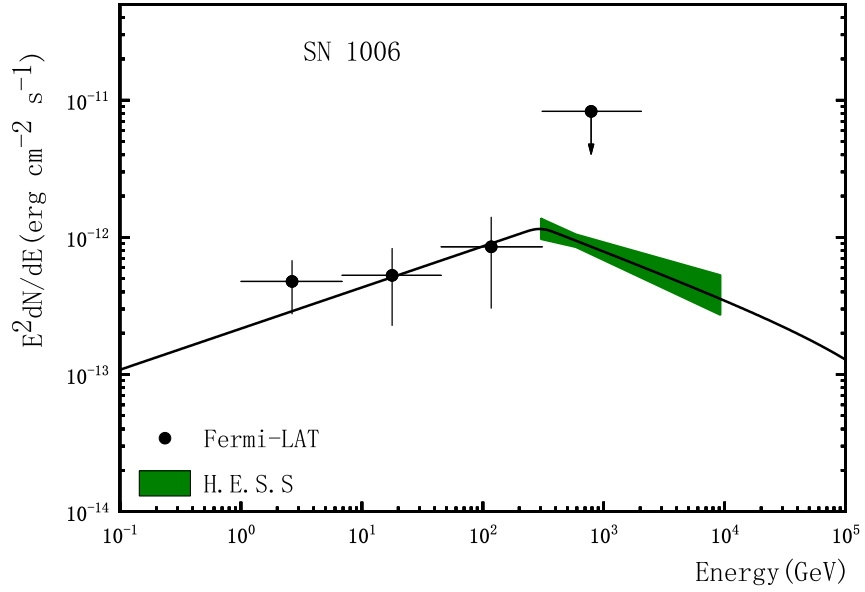


Figure 9: Predicted gamma ray spectrum multiplied by  $E^2$  and comparisons with the H.E.S.S. and Fermi-LAT spectrum for SN 1006 [41]. The parameters see Table 1.

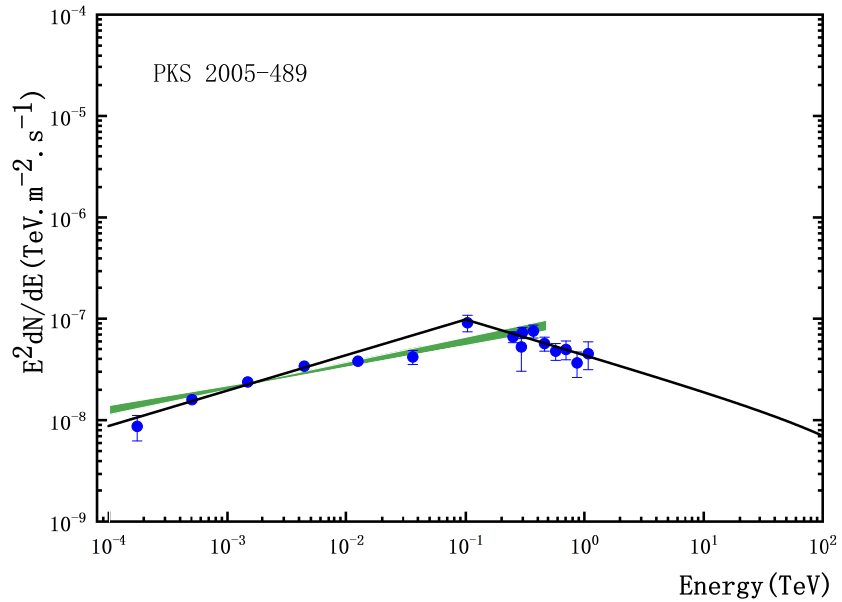


Figure 10: Predicted gamma ray spectrum multiplied by  $E^2$  and comparisons with the H.E.S.S. and Fermi-LAT spectrum for PKS 2005 [42]. The parameters see Table 1.

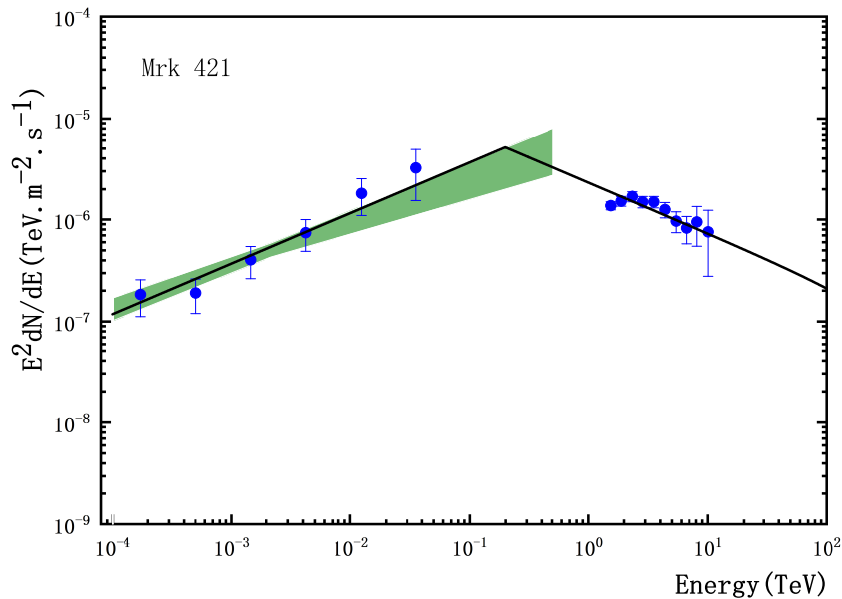


Figure 11: Predicted gamma ray spectrum multiplied by  $E^2$  and comparisons with the H.E.S.S. and Fermi-LAT spectrum for Mrk 421 [42]. The parameters see Table 1.

distribution's exponential tail in the cascade model. The result of Telescope Array has not found a big increment effect in  $\sigma_{p-air}$  till  $\sqrt{s} = 95$  TeV [46,47]. However, the cascade method has the fundamental limitation. Some of important parameters are undetermined [48]. Besides, the GC-effects may disappear quickly at the beginning collisions due to the energy loss of the leading proton. Therefore, we do not regard the Telescope Array data as a restriction to the value of  $E_{\pi}^{GC}$  in this work

The GC-threshold  $E_{p-p(A)}^{GC}$  is target-dependent. Because the nonlinear term of the QCD evolution equation should be re-scaled by  $A^{1/3}$ ,  $E_{\pi}^{GC}$  decreases with increasing A [2]. High energy protons may collide with nuclei in Universe. The GC-threshold decreases in high dense (or heavy nuclear) matter [2,3]. Therefore,  $E_{p-A}^{GC} < E_{p-p}^{GC}$  is expected. A-dependence of  $E_{p-A}^{GC}$  is a complicated problem, which relates to the distribution and structure of the GC-source. In this work we use the experimental data to determine the values of  $E_{p-p(A)}^{GC}$  (or  $E_{\pi}^{GC}$ ). However, we should point out that (i) not all elements

show their GC-effects, some of them will be shadowed by the background due to lower abundance or suppression factors in the propagation.

## 5 The GC-effects in the electron-positron spectra

High energy photons via  $p + p(A) \rightarrow \pi$  and  $\pi^0 \rightarrow \gamma$  through strong electric field inside source, they may product electron/ positron pair.

Considering the protons are accelerated to beyond the GC-threshold inside a strong source (for say, supernova remnant). The primary product of hadronic processes is the production of pion via

$\pi = (\pi^+, \pi^0, \pi^-)$ . Then we have  $\pi^\pm \rightarrow \mu^\pm + \nu_\mu(\bar{\nu}_\mu)$ ,  $\mu^\pm \rightarrow e^\pm + \nu_e(\bar{\nu}_e) + \bar{\nu}_\mu(\nu_\mu)$  and  $\pi^0 \rightarrow 2\gamma$ . We focus the electron/positron pair cascades  $\gamma + magnetic\ field \rightarrow e^+ + e^-$  in the source. We use the hadronic model to calculate the electron/positron spectra, which is combined by includes the following factors: the spectrum of injection proton  $E_{p-p(A)}^{-\beta_p}$ ,  $\pi$ -spectrum  $N_\pi$  at  $p-p(A)$  collisions beyond the GC-threshold, the probabilities of  $\pi^0 \rightarrow \gamma$  and  $\gamma \rightarrow e^- + e^+$ , the electron/positron propagation effects  $E_j^{-\beta_j}$ . The isotropic measured electron and positron fluxes are

$$\Phi_j(E_j) = \Phi_j^0(E_j) + \Phi_j^{GC}(E_j), \quad (15)$$

for  $j = e^-$  or  $e^+$  and

$$\begin{aligned} \Phi_j^{GC}(E_j) &= C_j \left( \frac{E_j}{E_0} \right)^{-\beta_j} \int_{E_j} dE_\gamma \left( \frac{E_\gamma}{E_0} \right)^{-\beta_\gamma} \int_{E_\pi^{min}}^{E_\pi^{max}} dE_\pi \left( \frac{E_{p-p(A)}}{E_{p-p(A)}^{GC}} \right)^{-\beta_p} \\ &\quad N_\pi(E_{p-p(A)}, E_\pi) \frac{d\omega_{\pi-\gamma}(E_\pi, E_\gamma)}{dE_\gamma} \frac{d\omega_{\gamma-e}(E_\gamma, E_e)}{dE_e} \\ &= C_j \left( \frac{E_j}{E_\pi^{GC}} \right)^{-\beta_j} \int_{E_j} \frac{dE_\gamma}{E_\gamma} \left( \frac{E_\gamma}{E_\pi^{GC}} \right)^{-\beta_\gamma} \int_{E_\pi^{GC} \text{ or } E_\gamma}^{E_\pi^{max}} dE_\pi \left( \frac{E_{p-p(A)}}{E_{p-p(A)}^{GC}} \right)^{-\beta_p} N_\pi(E_{p-p(A)}, E_\pi) \frac{2}{\beta_\pi E_\pi} \\ &= \begin{cases} \frac{50C_j}{2\beta_p-1} E_\pi^{GC} \left( \frac{E_j}{E_\pi^{GC}} \right)^{-\beta_j} \left[ \frac{1}{\beta_\gamma} \left( \frac{E_j}{E_\pi^{GC}} \right)^{-\beta_\gamma} + \left( \frac{1}{\beta_\gamma+2\beta_p-1} - \frac{1}{\beta_\gamma} \right) \right] & \text{if } E_j \leq E_\pi^{GC} \\ \frac{50C_j}{(2\beta_p-1)(\beta_\gamma+2\beta_p-1)} (E_\pi^{GC}) \left( \frac{E_j}{E_\pi^{GC}} \right)^{-\beta_j-\beta_\gamma-2\beta_p+1} & \text{if } E_j > E_\pi^{GC} \end{cases} \quad (16) \end{aligned}$$

where the integral lower-limit takes  $E_\pi^{GC}$  (or  $E_\gamma$ ) if  $E_\gamma \leq E_\pi^{GC}$  (or if  $E_\gamma > E_\pi^{GC}$ ). After taking average over possible directions, the energy of pair-produced electron-positron is

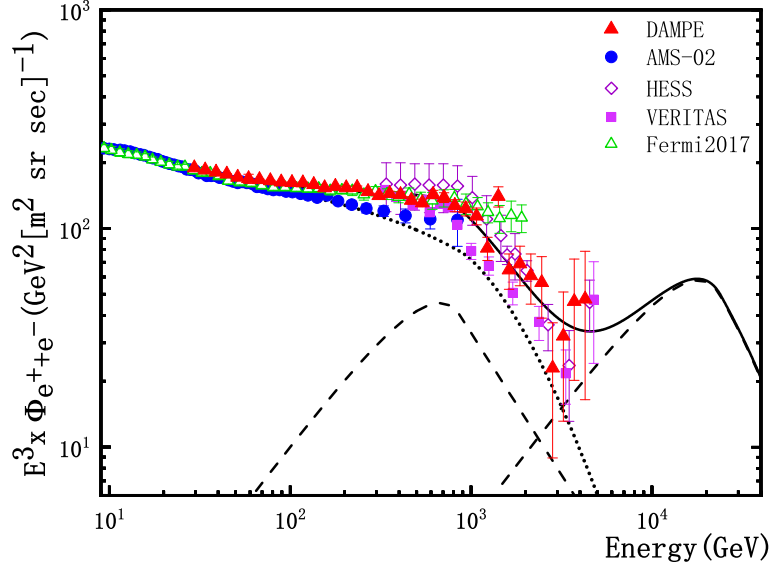


Figure 12: Predicted cosmic electron spectrum multiplied by  $E^3$  as a function of energy (solid curve). Broken curves present the broken power-law of the GC-effects. The data are taken from [1,4-7].

uniformly distributed from zero to maximum value, i.e.,

$$\frac{d\omega_{\gamma-e}(E_\gamma, E_e)}{dE_e} = \frac{1}{E_\gamma}. \quad (17)$$

In Eq. (16)  $N_\pi(E_{p-p(A)}, E_\pi)$  is calculated using Eq. (5);  $E_{p-p(A)}$  is the energy of incident proton in the rest frame of targeted proton. Equation (16) shows the electron spectrum is smoothly broken at  $\sim E_\pi^{GC}$ .

Figure 12 is a result fitting data including the DAMPE spectrum, where using  $E_\pi^{GC} = 880$  GeV for  $p-A$  collisions and  $E_\pi^{GC} = 24$  TeV for  $p-p$  collisions, respectively.  $\Phi_{e^+e^-}^0$  is refers to [49], where we reduce the background line to lower than the data at  $E > 1$  TeV. The data are taken from [49-52]. The parameters  $E_\pi^{GC} = 880$  GeV,  $\beta_p = 1.7$ ,  $\beta_\gamma = 1.3$ ,  $\beta_e = 0.6$ ,  $C_{880 \text{ GeV}} = 1.15 \times 10^{-6}$  and  $C_{24 \text{ TeV}} = 3.6 \times 10^{-9}$ . The results present a smoothly broken power at 0.9 TeV and the curve is turning again at  $3 \sim 4$  TeV. Usually, the power index  $\beta_e \sim 2-3$ . The production mechanism of electron/positron is separated by  $d\omega_{\gamma-e}/dE_e$ . Therefore, the above smaller index is accepted.



For understanding the GC-effects in this example, we image the case without the GC-effects. The gamma-ray spectrum from  $p+p \rightarrow \pi^0 \rightarrow 2\gamma$  will peak at  $\sim 1$  GeV and it has been proved [33,34]. In this case, the following contributions of  $\gamma \rightarrow e^+ + e^-$  at tail ( $> 100$  GeV) to the electron-flux are much lower than the background and they are completely negligible.

Why the GC-threshold  $E_{p-A}^{GC}$  (or  $E_{\pi}^{GC}$ ) of gamma-ray spectra is more abundant than that of electron-positron spectra. The reason is that the observed charged cosmic rays on the Earth origin mainly from the nearest galaxy-milky way. Most electron/positron origin from extragalactic galaxies (AGNs) and they are suppressed due to radiation in long distance transmission.

In concretely, we assume that the GC-threshold at  $p-Pb$  collisions is  $E_{p-Pb}^{GC} = 3.4 \times 10^7$  GeV or  $\sqrt{s_{p-Pb}^{GC}} = \sqrt{s_{Pb-Pb}^{GC}} = 8$  TeV. Thus, we suggest that  $E_{\pi}^{GC} \simeq 1$  TeV in electron/positron spectra origins from proton-intermediate nucleus. While the GC-threshold  $E_{\pi}^{GC} \ll 1$  TeV in gamma ray spectra may arise from proton-heavy nucleus collision or proton-(head-on) moving nucleus. In the later case, the effective GC-threshold is reduced.

A large amount of pions with a certain energy accumulate in a narrow space at per collision, they may transform each other in the formation time due to their wave-functions overlap, i.e.,  $\pi^+ + \pi^- \rightleftharpoons 2\pi^0$ . However, the above balance will be broken since  $m_{\pi^+} + m_{\pi^-} > 2m_{\pi^0}$ , and the lifetime of  $\pi^0$  ( $10^{-16}$  s) is much shorter than the typical weak decay lifetimes of  $\pi^{\pm}$  ( $10^{-6}$  s –  $10^{-8}$  s). Therefore we neglect temporarily the contributions of  $\pi^{\pm}$ . The valid of this assumption will be checked by the following discussions

Now we consider the contributions of  $\pi^{\pm} \rightarrow \mu^{\pm} + \nu_{\mu}(\bar{\nu}_{\mu})$  and  $\mu^{\pm} \rightarrow e^{\pm} + \nu_e(\bar{\nu}_e) + \bar{\nu}_{\mu}(\nu_{\mu})$ , although this process is negligible as discussed above. Similar to Eq. (16), we have

$$\Phi_e^{GC}(E_e) = C_e \left( \frac{E_e}{1 \text{ GeV}} \right)^{-\beta_e} \int dE_{\mu} \int_{2.5E_e \text{ or } E_{\pi}^{GC}}^{E_{\pi}^{max}} \frac{dE_{\pi}}{E_{\pi}} \left( \frac{E_{p-p(A)}}{E_{p-p(A)}^{GC}} \right)^{-\beta_p} N_{\pi^{\pm}}(E_{p-p(A)}, E_{\pi})$$

$$\frac{d\omega_{\pi-\mu}(E_\pi, E_\mu)}{dE_\mu} \frac{d\omega_{\mu-e}(E_\mu, E_e)}{dE_e} = \begin{cases} \frac{370C_e}{2\beta_p-1} E_e^{GC} \left(\frac{E_e}{E_e^{GC}}\right)^{-\beta_e+2} & \text{if } E_e \leq E_e^{GC} \\ \frac{370C_e}{2\beta_p-1} E_e^{GC} \left(\frac{E_e}{E_e^{GC}}\right)^{-\beta_e-2\beta_p+2} & \text{if } E_e > E_e^{GC} \end{cases}, \quad (18)$$

where the normalized spectra are

$$\frac{d\omega_{\pi-\mu}(E_\pi, E_\mu)}{dE_\mu} = \delta(E_\mu - 0.8E_\pi), \quad (19)$$

and

$$\frac{d\omega_{\mu-e}(E_\mu, E_e)}{dE_e} = 4\left(\frac{2E_e}{E_\mu}\right)^2\left(1.5 - \frac{2E_e}{E_\mu}\right), \quad E_e \leq \frac{E_\mu}{2}. \quad (20)$$

The results are shown in Fig. 13, where we take break energy  $E_e^{GC} \sim 1.4$  TeV. The spectrum in Fig. 13 presents a sharp broken power-law, which is different from a smoothed broken power at  $E_\pi^{GC} \sim 0.9$  TeV. The reason is that the integral of  $E_\gamma$  in Eq. (16) smooths the corner, while Eq. (14) lacks such smooth factor. .

The angle at 1.4 TeV may become more smaller if we assume that there is dense gas around this GC-source. In this case, a larger diffusion index will be incorporated into the index  $\beta_p$  in Eq. (19) when the injected protons crossing the dense gas region. On the other hand, a suppressed factor  $B$  should be inserted into Eq. (19), which describes that a part of lower energy electrons are stopped in the dense gas. Figure 14 shows a result. This example shows that a sharp peak at the TeV-band seems permissible. However, as we have mentioned that the probability of  $\pi^\pm$  decay is much smaller than that of  $\pi^0$  decay due to the accumulation of pions at  $p-p(A)$  collisions. Therefore, we suggest that the sharp structure is appeared as a rare event and it maybe mixed with random fluctuations in the measurements.

The positron spectrum could show GC-signature clearer because a very low  $e^+$ -background. The electron and positron have an equal creation probability from  $\gamma \rightarrow e^+ + e^-$ , i.e.,

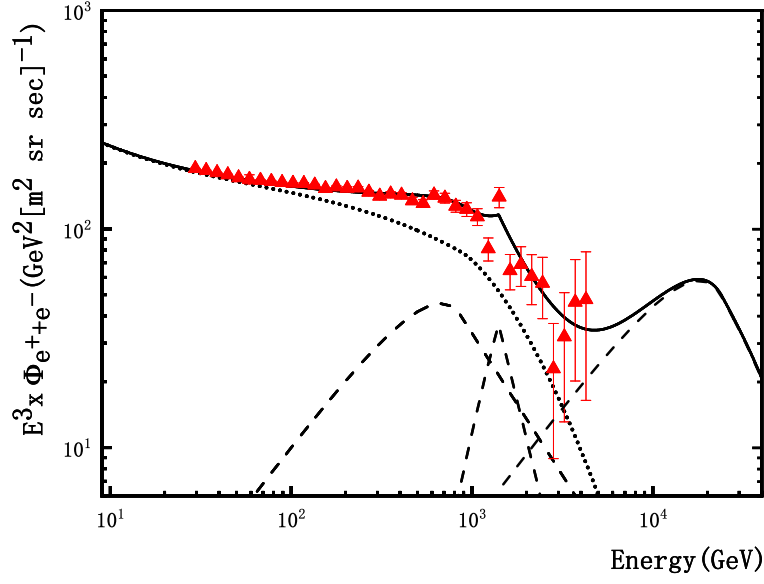


Figure 13: As similar to Fig. 12 but added the corrections of Eq. (3.5). The added parameters for the peak at 1.4  $TeV$ :  $\beta_p = 3.9$ , which incorporates the index of  $\pi^\pm$ ,  $\beta_e = 0.6$  and  $C_{1.4 TeV} = 5.0 \times 10^{-15}$ . The data are taken from the DAMPE [47].

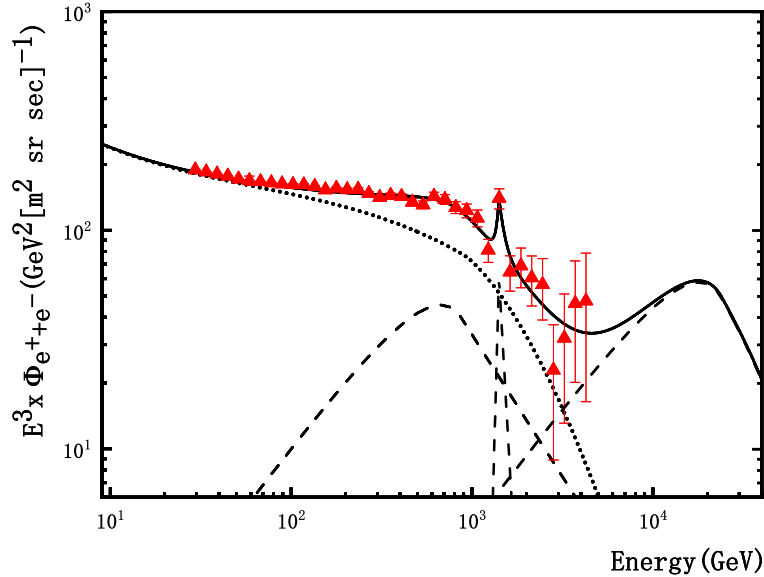


Figure 14: Similar to Fig. 13 but added a suppression factor  $B = \theta(1.4 - E_e) \exp(-0.2 \times (1.4 - E_e))$  in GeV unit and a larger effective  $\beta_p = 3.9 + 5.6$  are used due to the corrections of the imaginary dense gas around this GC-source.

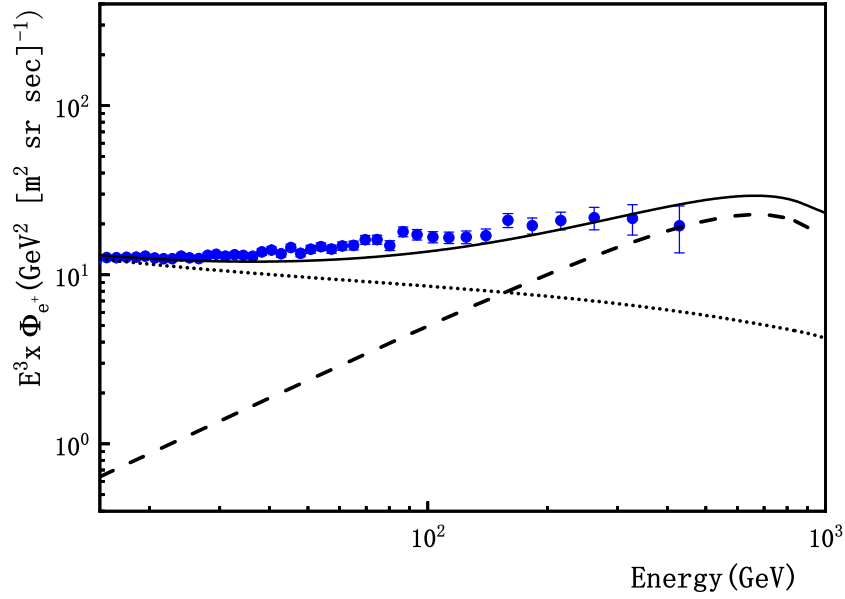


Figure 15: Predicted positron spectrum multiplied by  $E^3$  as a function of energy. The data are taken from [53-56].

$$\Phi_{e^+}^{GC}(E_e) = \frac{1}{2}\Phi_{e^-+e^+}^{GC}(E_e). \quad (21)$$

However, the background of positron flux is much lower than that of electron flux in sky. It originates from the unknown cosmic evolution. Unfortunately, we lack the data of positron background, which is model-dependent. We take a simple assumption, i.e.,

$$\Phi_{e^+}^0(E_e) = \eta\Phi_{e^-+e^+}^0(E_e). \quad (22)$$

$\eta = 0.06$  is determined by the value of  $\Phi_{e^+}(E_e)$  at  $E_e = 20$  GeV, where there is no GC-effects. Our predicted positron flux using Eqs. (16), (21) and (22) without other extra parameters is shown in Fig. 15. The data are taken from [53-56]. Now we can conclude that the increment of secondary particles due to the GC-effects can explain the observed broken power-law in electron and positron spectra, although the positron background has uncertainty.

## 6 Summary

A new discovery in QCD is that the gluons in proton may converge to a state with a critical momentum at a high energy range. This gluon condensation (GC) increases suddenly the proton-proton or proton-nuclei cross sections. A natural suggestion is that many observed, but uncomprehended excesses in cosmic ray spectra origin from a common source-the GC. We find that the GC-effects in  $p - p(A) \rightarrow \pi^0 \rightarrow \gamma$  sharply break the gamma spectra. We present three possible broken power-laws of eletron/positron spectra around  $\sim 1$  TeV: a smooth break and the sharp beaks with different sharpness using the GC-effects. The relating excess of positron is also discussed. The GC is a new phenomenon that is not yet known, it provides a new window to understand the high energy cosmic ray spectra.

**Acknowledgments:** *Acknowledgments:* This work is supported by the National Natural Science of China (No.11851303). We thank X.R. Chen, L. Feng, D.B. Liu, P.M. Zhang and Y.P. Zhang for useful discussions.

## References

- [1] W. Zhu, Z.Q. Shen and J.H. Ruan, *Chin. Phys. Lett.* **25** (2008) 3605.
- [2] W. Zhu, Z.Q. Shen and J.H. Ruan, *Nucl. Phys. B* **911** (2016) 1.
- [3] W. Zhu and J. Lan, *Nucl. Phys. B* **916** (2017) 647.
- [4] S. Archambault et. al., *Astrophys. J.* **836** (2017) 23.
- [5] M. Aguilar et al., *Phys. Rev. Lett.* **113** (2014) 121102.
- [6] J. Chang, et al., *Nature* **456** (2008) 362.
- [7] A. A. Abdo et al., *Phys. Rev. Lett.* **102** (2009) 181101.
- [8] F. Aharonian et al., *Phys. Rev. Lett.* **101** (2008) 261104.
- [9] F. Aharonian et al., *Astron. Astrophys.* **508** (2009) 561.
- [10] D. B. Tridon, et al., Proc. of the 32nd ICRC [arXiv:hep-ph/1110.4008].
- [11] D. Staszak, for the VERITAS Collaboration, A Cosmic-ray Electron Spectrum with VERITAS, 2015, To appear in the Proceedings of the 34th International Cosmic Ray Conference (ICRC2015), The Hague, The Netherlands (PoS ICRC 411) [arXiv:astro-ph/1508.0659].
- [12] V.N. Gribov and L.N. Lipatov, *Sov. J. Nucl. Phys.* **15** (1972) 438.
- [13] Yu.L. Dokshitzer, *Sov. Phys. JETP.* **46** (1977) 641.
- [14] G. Altarelli and G. Parisi, *Nucl. Phys. B* **B126** (1977) 298.
- [15] L. N, Lipatov, *Sov. J. Nucl. Phys.* **23** (1976) 338.
- [16] V. S. Fadin, E.A. Kuraev and L. N. Lipatov, *Phys. Lett. B* **60** (1975) 50.

- [17] E. A. Kuraev, L.N. Lipatov and V. S. Fadin, *Sov. Phys. JETP*. **44** (1976) 443.
- [18] E. A. Kuraev, L.N. Lipatov and V. S. Fadin, *Sov. Phys. JETP*. **45** (1977) 199.
- [19] I.I. Balitsky and L.N. Lipatov, *Sov. J. Nucl. Phys.* **28** (1978) 622.
- [20] L.V. Gribov, E.M. Levin and M.G. Ryskin, *Phys. Rep.* **100** (1983) 1.
- [21] A.H. Mueller and J. Qiu, *Nucl. Phys. B* **268** (1986) 427.
- [22] W. Zhu, *Nucl. Phys. B* **551** (1999) 245 [arXiv:hep-ph/9809391].
- [23] W. Zhu, J.H. Ruan, *Nucl. Phys. B* **559** (1999) 378 [arXiv:hep-ph/9907330].
- [24] W. Zhu and Z.Q. Shen, *HEP & NP*, **29** (2005) 109.
- [25] I. Balitsky, *Nucl. Phys. B* **463** (1996) 99.
- [26] Yu. Kovchegov, *Phys. Rev. D* **60** (1999) 034008.
- [27] J. Jalilian-Marian, A. Kovner, L. McLerran, and H. Weigert, *Phys. Rev. D* **55** (1977) 5414.
- [28] J. Jalilian-Marian, A. Kovner, A. Leonidov, and H. Weigert, *Nucl. Phys. B* **504** (1977) 415.
- [29] H. Weigert, *Nucl. Phys. A* **703** (2002) 823.
- [30] W. Zhu, J.H. Ruan, J.F. Yang, and Z.Q. Shen, *Phys. Rev. D* **68** (2003) 094015.
- [31] J.H. Ruan and W. Zhu, *Phys. Rev. C* **80** (2009) 045209.
- [32] J.H. Ruan and W. Zhu, *Phys. Rev. C* **81** (2010) 055209.
- [33] W. Zhu, J.H. Ruan and F.Y. Hou, *Int. J. Mod. Phys. E* **22** (2013) 1350013.

- [34] X.R. Chen, J.H. Ruan, R. Wang, P.M. Zhang and W. Zhu, *Int. J. Mod. Phys. E* **23** (2014) 145005.
- [35] W. Zhu and J.H. Ruan *Int. J. Mod. Phys. E* **E24** (2015) 1550077.
- [36] V.V. Anisovch, M.N. Kobrinsky, J. Nyiri and Y.M. Shabelski, Quark model and high energy collisions, World Scientific Publishing (1985).
- [37] Q. Wang and Q.B. Xie, *Phys. Rev. D* **52** (1995) 1469.
- [38] T.K. Gaisser, Cosmic Rays and Particle Physics, The press Syndicate of the University of Cambridge 1990.
- [39] M. Ackermann, et al. *Science*, **339** (2013) 807.
- [40] C. D. Dermer, et. al., [arXiv:astro-ph/1303.6482].
- [41] H.E.S.S. Collab. (D. Zaborov et al.), [arXiv:astro-ph/1612.05111].
- [42] B. Condon, M. Lemoine-Goumard, F. Acero and H. Katagiri, [arXiv:astro-ph/1711.05499].
- [43] H.E.S.S. Collab. (C. Romoli et al.), [arXiv:astro-ph/1708.01153v2].
- [44] K. Greisen, *Phys. Rev. Lett.* **16** (1966) 748.
- [45] G. T. Zatsepin and V. A. Kuzmin, *JETP. Lett.* **4** (1966) 78.
- [46] W. Hanlon and R. Abbasi, Presented at EDS Blois 2017, Prague, Czech Republic, June 26-30, 2017 [arXiv:astro-ph/1711.00060].
- [47] R. Abbasi and G. Thomson, Proc. 2016 Int. Conf. Ultra-High Energy Cosmic Rays (UHECR2016), JPS Conf. Proc. , (2018) 011015.



- [48] T.K. Gaisser, Cosmic Rays and Particle Physics, The press Syndicate of the University of Cambridge 1990.
- [49] DAMPE Collab. (G. Ambrosi et al.), *Nature*, 552 (2017) 63.
- [50] Q. Yuan et. al., [arXiv:astro-ph/1711.10989].
- [51] AMS Collab. (M. Aguilar et al.), *Phys. Rev. Lett.* 117 (2016) 091103.
- [52] Fermi LAT Collab. (S. Abdollahi et al.), *Phys. Rev.* **D95**, 082007 (2017).
- [53] H.E.S.S. Collab. (F. Aharonian<sup>1</sup> et al.), *Astron. Astrophys.* 508 (2009) 561, arXiv:astro-ph/0905.0105].
- [54] M. Aguilar, et al., *Phys. Rev. Lett.* **113** (2014) 121102.
- [55] O. Adriani, et al., *Phys. Rev. Lett.* **111** (2013) 081102.
- [56] O. Adriani, et al., *Phys. Rev. Lett.* **105** (2010) 121101.